RESEARCH ARTICLE

The Genetic Landscape and Clonal Evolution of Breast Cancer Resistance to Palbociclib plus Fulvestrant in the PALOMA-3 Trial

Ben O'Leary[1,2], Rosalind J. Cutts[1], Yuan Liu[3], Sarah Hrebien[1], Xin Huang[3], Kerry Fenwick[4], Fabrice André[5], Sibylle Loibl[6], Sherene Loi[7], Isaac Garcia-Murillas[1], Massimo Cristofanilli[8], Cynthia Huang Bartlett[3], and Nicholas C. Turner[1,2]

ABSTRACT CDK4/6 inhibition with endocrine therapy is now a standard of care for advanced estrogen receptor–positive breast cancer. Mechanisms of CDK4/6 inhibitor resistance have been described preclinically, with limited evidence from clinical samples. We conducted paired baseline and end-of-treatment circulating tumor DNA sequencing from 195 patients in the PALOMA-3 randomized phase III trial of palbociclib plus fulvestrant versus placebo plus fulvestrant. We show that clonal evolution occurs frequently during treatment, reflecting substantial subclonal complexity in breast cancer that has progressed after prior endocrine therapy. *RB1* mutations emerged only in the palbociclib plus fulvestrant arm and in a minority of patients (6/127, 4.7%, $P = 0.041$). New driver mutations emerged in *PIK3CA* ($P = 0.00069$) and *ESR1* after treatment in both arms, in particular *ESR1* Y537S ($P = 0.0037$). Evolution of driver gene mutations was uncommon in patients progressing early on palbociclib plus fulvestrant but common in patients progressing later on treatment. These findings inform future treatment strategies to address resistance to palbociclib plus fulvestrant.

SIGNIFICANCE: Acquired mutations from fulvestrant are a major driver of resistance to fulvestrant and palbociclib combination therapy. *ESR1* Y537S mutation promotes resistance to fulvestrant. Clonal evolution results in frequent acquisition of driver mutations in patients progressing late on therapy, which suggests that early and late progression have distinct mechanisms of resistance. *Cancer Discov; 8(11); 1390–403. ©2018 AACR.*

See related commentary by Schiff and Jeselsohn, p. 1352.

INTRODUCTION

Selective cyclin-dependent kinase 4 and 6 (CDK4 and CDK6) inhibitors have become the standard of care for advanced, estrogen receptor–positive (ER^+), and HER2-negative metastatic breast cancer (1). Estrogen and oncogenic signaling increases cellular levels of the D-type cyclins, particularly cyclin D1, activating CDK4 and CDK6 in a process modulated by the INK4A protein family, which includes p16, p21, and p27 (2). Activated CDK4/6 phosphorylates retinoblastoma (RB), in turn partially activating the E2F transcription factors, which promote S phase entry in a positive feedback loop involving cyclin E and CDK2 (3, 4). Multiple phase III studies have now demonstrated that CDK4/6 inhibitors significantly prolong progression-free survival (PFS) in combination with endocrine therapy in ER-positive breast cancer (5–8), identifying the CDK4/6–RB axis as central to the biology of this subtype of breast cancer.

With CDK4/6 inhibitors now a standard of care, it is critical to identify the mechanisms of resistance to therapy and develop treatment strategies after clinical progression. A number of putative resistance mechanisms to CDK4/6 inhibition have been identified in preclinical models: *RB1* loss, cyclin E1 and cyclin E2 amplification (9), and *CDK6* amplification (10). Clinical evidence is limited, with a case report of *RB1* mutations in 3 patients treated with CDK4/6 inhibitors (11), but no systematic assessment of resistance mechanisms. Mutations in *RB1* are rare in primary breast cancer (12), but the prevalence of these in endocrine-pretreated and CDK4/6 inhibitor–resistant breast cancer is unknown. Loss-of-function *RB1* mutations may render the tumor resistant to subsequent endocrine-based therapies or prevent benefit from continuing CDK4/6 inhibitors beyond progression, so identifying how frequently the tumor acquires *RB1* mutations is important in planning trials of post-CDK4/6 therapy. In addition, prior data have suggested that common genomic aberrations such as *PIK3CA* mutations and *ESR1* mutations have limited value as a biomarker for CDK4/6 inhibitor treatment (13).

Here, we provide a comprehensive assessment of the genetic aberrations of CDK4/6 inhibitor–resistant disease using circulating tumor DNA (ctDNA) analysis of paired baseline and end-of-treatment (EOT) plasma samples from the PALOMA-3 study. The PALOMA-3 study was the first phase III trial of a CDK4/6 inhibitor in ER^+, $HER2^-$ advanced breast cancer, randomizing both premenopausal and postmenopausal patients who had previously progressed on endocrine therapy to either palbociclib plus fulvestrant or placebo plus fulvestrant, and demonstrating an improvement in median PFS from 4.6 to 11.2 months with the addition of palbociclib to fulvestrant (14), updated in ref. 15. Analysis of paired samples from this randomized study allows a dissection of which genetic events are acquired through therapy, specifically which component of the combination therapy may be driving selection of the mutations. Acquired mutations

[1]Breast Cancer Now Research Centre, The Institute of Cancer Research, London, United Kingdom. [2]Breast Unit, Royal Marsden Hospital, London, United Kingdom. [3]Pfizer, New York, New York. [4]Tumour Profiling Unit, The Institute of Cancer Research, London, United Kingdom. [5]Department of Medical Oncology, Institut Gustave Roussy, Villejuif, France. [6]German Breast Group, Neu-Isenburg, Germany. [7]Division of Research and Cancer Medicine, University of Melbourne, Peter MacCallum Cancer Centre, Melbourne, Victoria, Australia. [8]Robert H. Lurie Comprehensive Cancer Center, Feinberg School of Medicine, Chicago, Illinois.

Note: Supplementary data for this article are available at Cancer Discovery Online (http://cancerdiscovery.aacrjournals.org/).

Corresponding Author: Nicholas C. Turner, Institute of Cancer Research and The Royal Marsden Hospital, London SW3 6JB, United Kingdom. Phone: 020-7153-5574; E-mail: Nick.Turner@icr.ac.uk

doi: 10.1158/2159-8290.CD-18-0264

observed only in the palbociclib plus fulvestrant group likely promote resistance to the CDK4/6 inhibitor, whereas acquired mutations at equal frequency in both groups likely promote resistance to fulvestrant and, in general, to endocrine therapy.

We demonstrate that *RB1* mutations arise following treatment with CDK4/6 inhibition, but that these mutations are likely subclonal and of relatively low prevalence, suggesting, in contrast to previous work, that they are not a major mechanism of resistance. Relatively frequent acquisition of new *PIK3CA* and *ESR1* mutations, in particular the *ESR1* Y537S mutation, in both treatment arms implicates these changes in the development of parallel mechanisms of resistance to the elements of combination treatment and suggests new avenues for therapy.

RESULTS

Exome Sequencing of Plasma DNA Reveals Clonal Evolution on Palbociclib plus Fulvestrant

From the 521 patients who were enrolled in the PALOMA-3 study, there were 459 patients with a baseline (day 1 of treatment) plasma sample available, 287 of these having a matched EOT (Supplementary Fig. S1). The patients with paired samples from this group had similar palbociclib benefit compared with the overall PALOMA-3 study population (Supplementary Fig. S2). Of patients without available matched EOT samples (n = 172), 94 had not progressed (94/172, 54.6%) compared with 74 in the matched set (74/287, 25.8%). We first identified paired day 1 and EOT samples for plasma DNA exome sequencing to achieve comprehensive assessment of progression of genetic events on palbociclib plus fulvestrant (Fig. 1A). To identify paired plasma samples with sufficient tumor purity for exome sequencing, we developed a novel copy-number and purity targeted sequencing strategy using a targeted amplicon panel that included approximately 1,000 single-nucleotide polymorphisms (SNP) in regions commonly lost in breast cancer (see Methods; Supplementary Fig. S3) and combined this with digital PCR data for *PIK3CA* and *ESR1* mutations (13). Using this approach, we identified 16 patients treated with palbociclib plus fulvestrant who had high tumor DNA purity in plasma (>10% tumor purity) at day 1 and EOT, with adequate material for exome library preparation (Supplementary Table S1). Of these, 9 of 16 (56.3%) patients had a *PIK3CA* mutation and 6 of 16 (37.5%) patients had an *ESR1* mutation in day 1 ctDNA. Five patients had matched germline DNA, and a further 3 additional unmatched germline DNA samples were also sequenced to expand the panel of germlines for filtering sequencing noise. As only 6 patients from the fulvestrant plus placebo arm had matched samples meeting the quality control criteria, these were not sequenced.

Plasma DNA underwent exome sequencing to a median depth of 164× (range, 139–212), with germline DNA sequenced to a median depth of 47× (range, 34–58; Supplementary Table S2). Two day 1 samples had evidence of contamination, and these pairs were excluded from comparative, paired analyses. The number of nonsynonymous variants detectable in the day 1 samples varied considerably among patients (range, 19–254; Supplementary Fig. S4). Analysis of the mutational signatures across all samples revealed the most prevalent were signatures 1 (age) and 3 (homologous recombination deficiency), consistent with existing data on breast cancer (ref. 16; Supplementary Table S3). Day 1 exome-sequencing data additionally revealed genetic markers potentially relevant to the development of endocrine resistance beyond *ESR1* mutations—mutations in the *NOTCH* family receptors *NOTCH2, NOTCH3,* and *NOTCH4* in 4 of 14 (28.6%) patients, and *NF1* mutations in 2 of 14 patients (14.3%; Supplementary Table S4). Genomic instability indices were broadly stable between day 1 and EOT for most patients, although, as seen with mutation burden, there was considerable variation among patients (Supplementary Fig. S5).

Clonal evolution and selection on palbociclib plus fulvestrant was clearly evident between day 1 and EOT plasma samples in 85.7% (12/14) of patients (Fig. 1; Supplementary Fig. S6). Patient 390 had two *RB1*-truncating mutations, p.Q257X and p.N519fs, that were detected only at EOT (Fig. 1B). Clonality analysis with PyClone (17) suggested these *RB1* mutations were in a resistant subclone, or potentially separate subclones with parallel evolution leading to phenotypic convergence, with a further treatment-sensitive subclone evident characterized by a *RUNXT1* mutation that regressed on treatment (Fig. 1C). Mutation counts per subclone as determined by the PyClone model were 155 (cluster 1), 64 (cluster 2), and 51 (cluster 3). The mutations in the resistant subclones were predominantly consistent with the APOBEC mutation signature (Fig. 1D; Supplementary Table S3). The *RB1* mutations were validated by digital PCR and confirmed to be absent at the start of treatment (Fig. 1E).

A second patient, 253, during treatment with palbociclib plus fulvestrant exhibited marked selection of a subclone featuring an activating mutation in the tyrosine kinase domain of *FGFR2* p.K569E, not detectable in the day 1 sample (Fig. 1F). Mutation counts per subclone, as determined by the PyClone

Figure 1. Paired ctDNA exome sequencing reveals frequent clonal selection on fulvestrant plus palbociclib. **A,** Day 1 and EOT plasma samples from the PALOMA-3 trial were screened using droplet digital PCR (ddPCR) and a targeted SNP sequencing approach to identify patients from the palbociclib plus fulvestrant arm who had paired plasma samples of sufficient tumor purity (>10%) for plasma exome sequencing. **B,** Paired ctDNA exome sequencing in patient 390 analyzed for clonal composition. A newly emergent *RB1*-mutant clone is detected at EOT, harboring two inactivating *RB1* mutations. **C,** Inferred phylogenetic tree of breast cancer from patient 390 derived from ctDNA. Yellow, truncal mutations present in all cancer cells; purple, subclone present at day 1 that subsequently regressed on treatment; gray, a newly emergent resistant clone characterized by two *RB1* mutations, arising separately to the purple subclone. **D,** Representation of mutational signatures identified in each individual subclone for patient 390. The raw data are shown in Supplementary Table S3. **E,** Digital PCR validation of the two *RB1* mutations Q257X and N519fs identified in the treatment-resistant subclone from patient 390. Results for day 1 and EOT are shown; Y axis, mutant probe amplitude; X axis, wild-type probe amplitude. **F,** Paired ctDNA exome sequencing in patient 253 analyzed for clonal composition. A new *FGFR2*-mutant clone undetectable at day 1 is detected at EOT. **G,** Inferred phylogenetic tree of breast cancer from patient 253 derived from ctDNA. Yellow, truncal mutations present in all cancer cells; purple, subclone characterized by an *ESR1* D538G mutation present at day 1 that subsequently regressed on treatment; orange, newly emergent resistant clone characterized by an *FGFR2* kinase domain mutation, arising separately from the purple subclone; gray, a subclone arising from the *FGFR2*-mutant subclone characterized by an *ESR1* Q75E mutation. **H,** Representation of mutational signatures identified in each individual clone from patient 253. The raw data are shown in Supplementary Table S3. **I,** Digital PCR validation of the *FGFR2* mutation from patient 253 showing results for plasma at day 1 and EOT. HR, homologous recombination; MMR, mismatch repair.

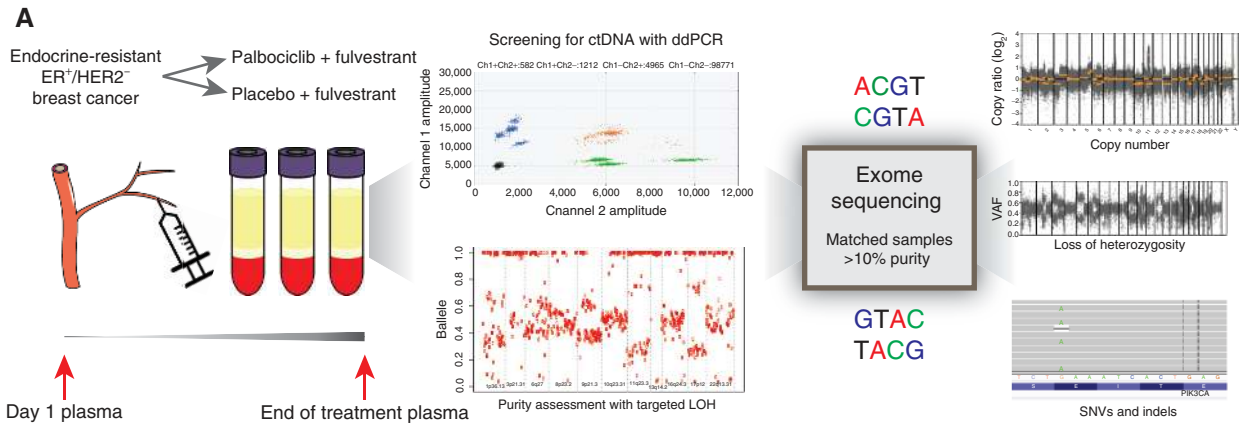

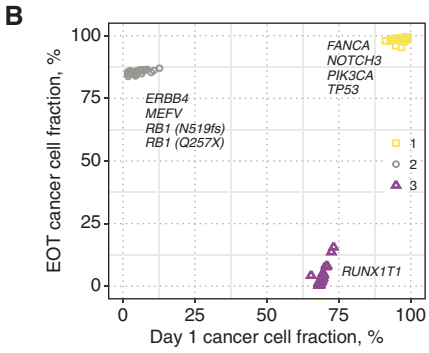

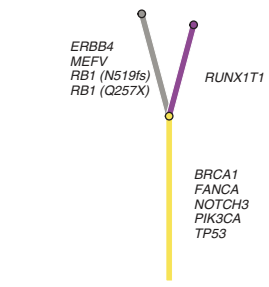

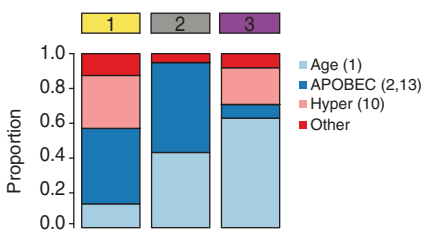

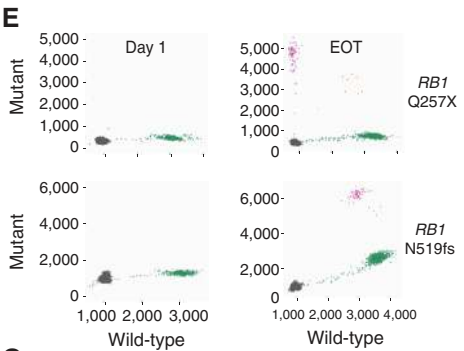

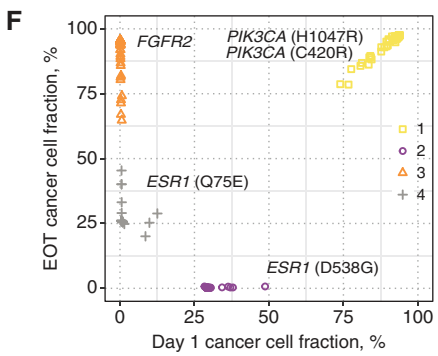

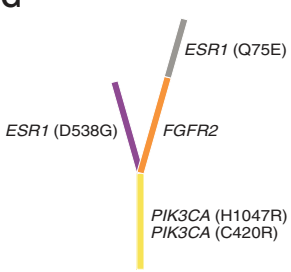

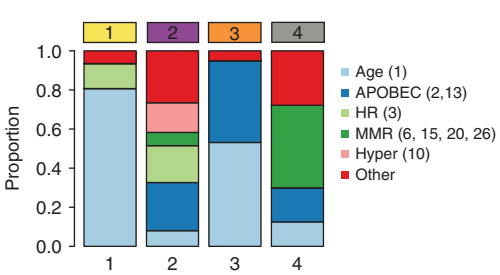

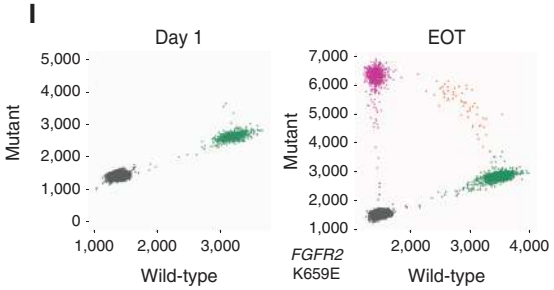

model, were 51 (cluster 1), 49 (cluster 2), 54 (cluster 3), and 20 (cluster 4). The newly dominant resistant subclone, with an additional *ESR1*-mutant Q75E daughter clone, replaced the day 1 *ESR1* D538G–mutant clone that was negatively selected by treatment (Fig. 1G). As Q75E is not a recognized cause of resistance to aromatase inhibitors and is positioned outside the ligand-binding domain of *ESR1*, these findings in this case suggest that changes in the dominant *ESR1* mutation between day 1 and EOT may reflect subclonal selection potentially unrelated to functional consequences of the *ESR1* mutation, with different *ESR1* mutations marking individual clones rather than potential emergence of the resistant clone. As seen with the resistant subclone in patient 390, the newly dominant *FGFR2*-mutant subclone in patient 253 also had a substantial proportion of mutations consistent with the APOBEC signature, with the minor daughter subclone mutations dominated by the mismatch repair signature (Fig. 1H; Supplementary Table S3). Selection of the *FGFR2* mutation was validated by digital PCR (Fig. 1I). In three further patients, there was possible evidence of selection of emergent mutations in antigen presentation pathways (Supplementary Table S4).

These findings demonstrate that clonal evolution is frequent in breast cancer on palbociclib plus fulvestrant, with evidence that the genomic plasticity of emergent subclones can be driven by different mutational processes from the bulk disease that is dominant at the start of treatment.

Patients Acquire New Driver Mutations in Both Treatment Arms

Paired exome sequencing findings were used to develop a targeted sequencing panel for error-corrected ctDNA sequencing of all available paired plasma samples, with DNA from each sample input into two separate library preparations and sequenced on two sequencing platforms with different fundamental chemistry, then compared together for final analysis to reduce both PCR error and sequencing error (see Methods). The targeted panel included all the coding exons of *RB1, CDK4, CDK6, CDKN1A, CDKN2B, NF1*, exons 5–8 of *TP53*, and known mutation hotspots in *PIK3CA, ESR1, ERBB2, FGFR1, FGFR2, FGFR3, AKT1, KRAS, NRAS,* and *HRAS*. *RB1* was included on the basis of the preexisting literature, with *FGFR1/2/3* and *NF1* added following the exome sequencing. In addition to the 14 patients with paired exome sequencing, libraries were generated from 206 patients at both day 1 and EOT for targeted sequencing (Supplementary Figs. S1 and S7). These underwent sequencing to median coverage of 2187× and 3251× for day 1 and EOT samples, respectively, on an Ion Proton, and to median coverage of 10637× and 8947× for day 1 and EOT samples on an Illumina HiSeq 2500, yielding 184 patients with paired sequencing data from both platforms meeting quality requirements (Methods; Supplementary Fig. S1). Combined with the paired exome sequencing this yielded 195 patients with paired ctDNA sequencing data (3 patients being included in both sets, Supplementary Fig. S1) to investigate selection on treatment with palbociclib plus fulvestrant ($n = 127$) or fulvestrant and placebo ($n = 68$).

Initially considering both treatment groups together, overall there were more mutations detected at EOT than at day 1, with 183 variant calls made in 105 patients at day 1 versus 243 variant calls in 119 patients at EOT (Fig. 2A). Sixty patients had at least one newly detectable/acquired mutation at the EOT (60/195, 30.8%). The acquisition of mutations at EOT did not appear to reflect low day 1 tumor content, as there were similar proportions of detected day 1 mutations in both patients with and without acquired mutations (35/60, 58.3% vs. 70/135, 51.9%, respectively). Additionally, there was no significant difference in the proportion of patients with >10% tumor purity at baseline (20.8% for patients with an acquired mutation, 31.0% for those without, $P = 0.21$, Fisher exact test), calculated using the SNP panel on a subset of $n = 163$ day 1 samples. There were similar proportions of patients in both treatment groups who acquired at least one new mutation, 39 of 127 (30.7%) in the palbociclib plus fulvestrant arm and 21 of 68 (30.9%) in the placebo plus fulvestrant arm.

Six patients acquired detectable *RB1* mutations at EOT ($P = 0.041$, McNemar test with continuity correction), all of these patients having received palbociclib plus fulvestrant. Two of these 6 patients had 2 *RB1* aberrations, 1 patient having been previously identified from the exome sequencing, suggesting polyclonal resistant subclones (Figs. 1C and 2B). The Q257X mutation identified in sample 418 was also validated with droplet digital PCR (ddPCR; Fig. 2B). In the 6 patients who acquired *RB1* aberrations, all 8 variants were either a gain of a stop codon or a frameshift deletion, highly likely to result in abrogated RB function. Four of the 6 patients who developed an *RB1* mutation also featured a *PIK3CA* mutation at a much higher allele fraction, suggesting that the *RB1* mutations could reflect subclones (Supplementary Fig. S8). Considering the two orthogonal sequencing approaches, amplicon and exome capture, similar EOT *RB1* mutation frequencies were identified in both at EOT in the palbociclib plus fulvestrant arm (exome sequencing 7.1%, 1/14; amplicon sequencing 3.9%, 5/127). These observations support the emergence of *RB1* aberrations being acquired or selected under pressure from palbociclib, but only in a minority of patients (6/127, 4.7%). Although we did not identify any *RB1* mutations at day 1, this is a chance result, as we identified 2 patients (in the fulvestrant plus placebo arm) with *RB1* mutations in a wider set of 331 day 1 samples that included patients without EOT samples.

Besides the emergence of *RB1* mutations on palbociclib, analysis of variants through treatment revealed different patterns across different genes, but a similar pattern between treatment groups (Fig. 2C). For *TP53,* there was predominantly persistence/maintenance of variants present at day 1 (Fig. 2A and C), consistent with variants in these genes commonly representing truncal changes. One patient with a day 1 *TP53* mutation acquired 8 newly detectable variants in *TP53* at EOT (Supplementary Fig. S9).

Selection of *PIK3CA* Mutations on Treatment

For *PIK3CA*, considering both treatment arms, 39 variants in 37 patients (37/195, 19.0%) were identified in the day 1 samples (Fig. 2A), consistent with previous findings (13) and indicating low levels of polyclonality. Almost all *PIK3CA* mutations present at day 1 were maintained after treatment (37/39, 95.7%), consistent with the majority of these being clonal/truncal mutations (Fig. 2C). At EOT, 55 *PIK3CA* variants in 52 patients from both treatment groups (52/195, 26.7%) were detected, an increase compared with day 1 (Fig. 2A; $P = 0.00069$, McNemar test). There was acquisition of *PIK3CA* mutations in 8.2% of patients overall (16/195), one of these acquiring

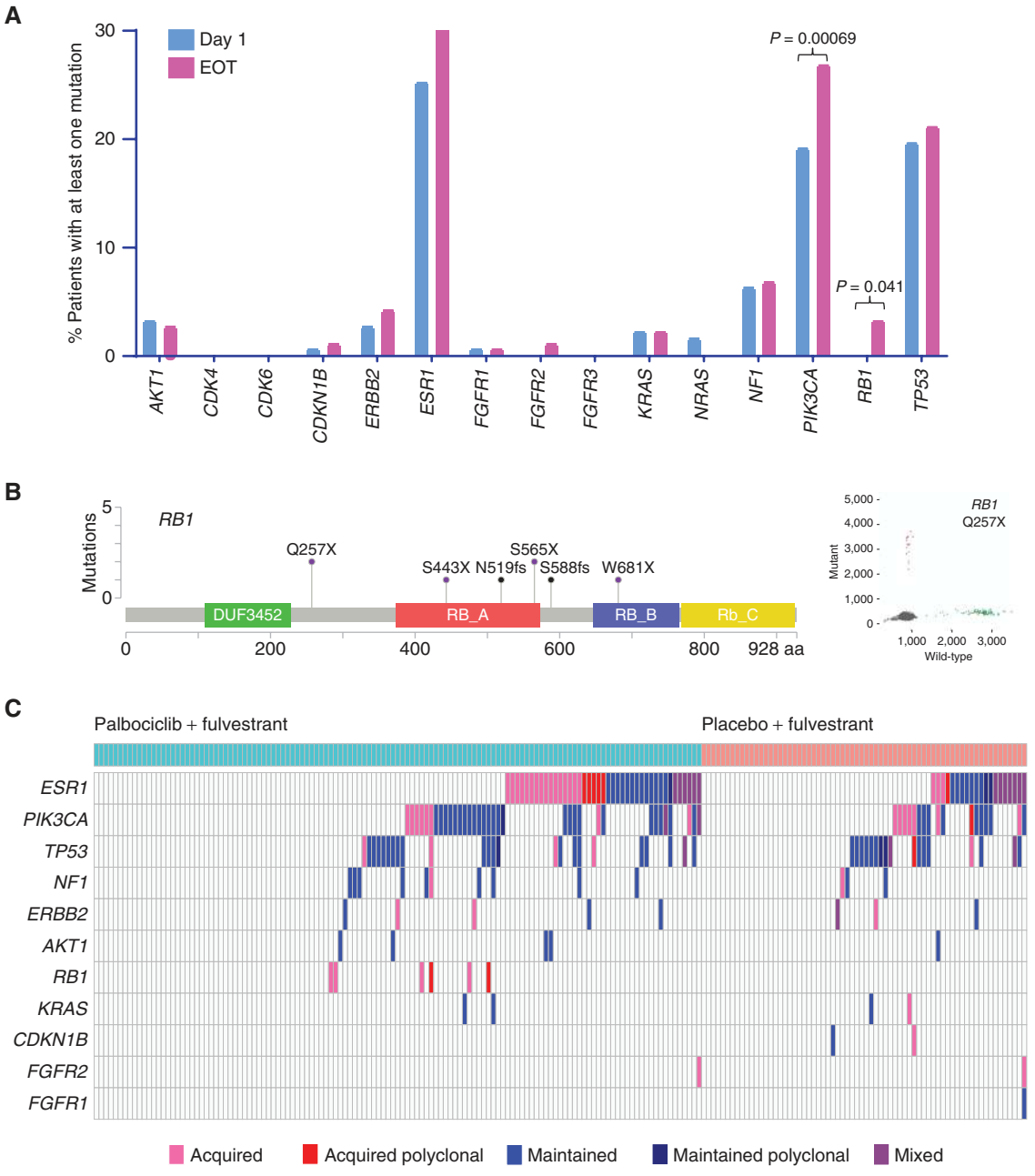

Figure 2. Genetic landscape of breast cancer driver genes in paired plasma samples on PALOMA-3 with frequent selection of mutations on treatment. **A,** Paired ctDNA sequencing results with frequency of observed variants in genes included in the targeted driver gene panel (SNVs and indels). Results are shown for both day 1 and EOT in 195 patients with matched data from day 1 and EOT. *P* values were calculated from the McNemar test with continuity correction. **B,** *RB1* mutations identified at EOT in patients treated with palbociclib plus fulvestrant (6/127). No *RB1* mutations were identified in the EOT plasma samples from patients treated with placebo and fulvestrant ($n = 68$). The digital PCR plot shows orthogonal validation of Q257X in the EOT sample from patient 418. **C,** EOT ctDNA sequencing results from 195 patients with paired samples, split by treatment, and whether the mutation status changed on treatment between day 1 and EOT. The cohort of 195 patients is formed from both the targeted sequencing cohort ($n = 184$) and exome-sequencing cohort ($n = 14$, with $n = 3$ in both sets; see Supplementary Fig. S1). The pattern of mutation acquisition is similar across both treatment arms. SNV, single-nucleotide variant; indel, insertion or deletion. Mixed, patients with different variants in the same gene at day 1 and EOT.

2 separate mutations and another acquiring an additional *PIK3CA* variant (Fig. 2C). The acquired *PIK3CA* mutations were validated with ddPCR for H1047R, H1047L, E545K, and E542K (the most common, accounting for 16/18 acquired variants) with 100% (16/16) of these validating and showing close agreement with the sequencing allele fraction estimation ($r = 0.97$; Supplementary Fig. S10). Considering specific *PIK3CA* mutations, there was some limited evidence for positive selection of E542K ($P = 0.041$, McNemar test with continuity correction; $q = 0.41$, Bonferroni correction; Supplementary

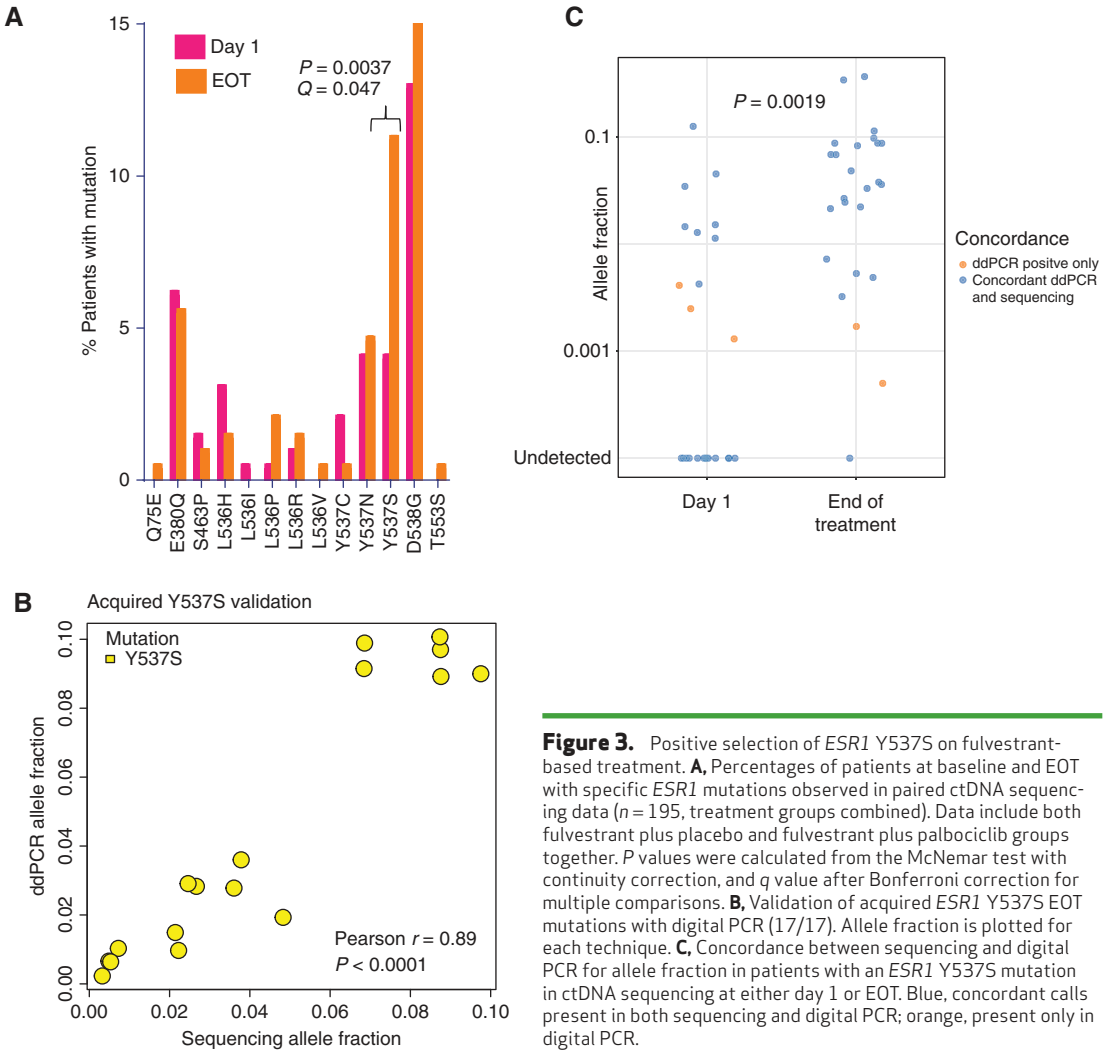

Figure 3. Positive selection of *ESR1* Y537S on fulvestrant-based treatment. **A,** Percentages of patients at baseline and EOT with specific *ESR1* mutations observed in paired ctDNA sequencing data ($n = 195$, treatment groups combined). Data include both fulvestrant plus placebo and fulvestrant plus palbociclib groups together. *P* values were calculated from the McNemar test with continuity correction, and *q* value after Bonferroni correction for multiple comparisons. **B,** Validation of acquired *ESR1* Y537S EOT mutations with digital PCR (17/17). Allele fraction is plotted for each technique. **C,** Concordance between sequencing and digital PCR for allele fraction in patients with an *ESR1* Y537S mutation in ctDNA sequencing at either day 1 or EOT. Blue, concordant calls present in both sequencing and digital PCR; orange, present only in digital PCR.

Fig. S11). Using digital PCR to test day 1 samples, a minority of the acquired *PIK3CA* mutations had the "acquired" mutation detectable at day 1 by digital PCR (6/18, 33.3%; Supplementary Fig. S12), with most of these at very low allele frequency below the limit of detection by ctDNA sequencing, providing evidence in some patients for outgrowth of a minor preexisting *PIK3CA*-mutant subclone. The increased proportion of *PIK3CA*-mutant patients at the EOT remained statistically significant in an analysis that included the digital PCR data at day 1 ($P = 0.016$, McNemar test). The proportion of patients acquiring newly detectable *PIK3CA* mutations did not appear to differ between treatment groups (Fig. 2C; Supplementary Figs. S13 and S14). These data are consistent with a proportion of initially *PIK3CA* wild-type tumors either positively selecting very low prevalence *PIK3CA*-mutant subclones or newly acquiring them on treatment with fulvestrant.

Selection of ESR1 Y537S on Treatment

ESR1 mutations were observed in 25.1% of patients at the start of treatment (49/195, 25.1%; Fig. 2A), with a similar overall number of patients with an *ESR1* mutation at the EOT (61/195, 31.3%, $P = 0.07$ McNemar test). However, 6.7% (13/195) of patients had an *ESR1* mutation detected at baseline and did not have an *ESR1* mutation detected at progression, and similarly 12.8% (25/195) of patients without an *ESR1* mutation detected at baseline had a newly acquired one at progression (Supplementary Fig. S14). Assessment of *ESR1* mutation status at baseline by digital PCR showed good overall agreement with the sequencing results (Supplementary Fig. S15).

Considering individual *ESR1* mutations, there was strong evidence for positive selection specifically of *ESR1* Y537S through treatment in both treatment groups ($P = 0.0037$, McNemar test; $q = 0.047$, Bonferroni correction; Fig. 3A). All of the acquired Y537S mutations were validated in the EOT samples by repeat testing with digital PCR (17/17; Fig. 3B). Considering the samples with a Y537S call in either time point, there was a minority of the acquired *ESR1* Y537S mutations that had the "acquired" mutation detectable at day 1 by digital PCR (3/17, 17.6%; Fig. 3C), providing evidence in some patients for outgrowth of a minor preexisting *ESR1* Y537S–mutant subclone. The increased proportion of *ESR1* Y537S–mutant patients at the EOT remained statistically significant in an analysis that included the digital PCR data at day 1 and EOT ($P = 0.0019$, McNemar test). An exploratory analysis of PFS

comparing patients with a Y537S mutation at day 1 to those who acquired Y537S by EOT showed a trend to significance despite the small numbers (log-rank $P = 0.011$; Supplementary Fig. S16). There were no clear differences in acquisition of specific *ESR1* mutations between treatment arms (Supplementary Fig. S17). Taken together, these data are consistent with *ESR1* Y537S promoting resistance to fulvestrant in the clinic.

Variants in further genes were acquired on treatment, including hotspot activating mutations in *ERBB2* (1.5%, 3/195), *KRAS* (0.5%, 1/195), and *FGFR2* (1.0%, 2/195), with no obvious difference in selection between treatment groups (Fig. 2C).

Clonal Evolution of Mutations with Treatment

We next contrasted the clonal changes observed in different genes across both treatment arms, separately considering the course of individual clones, and of patients with different combinations of subclones (Fig. 4A and B). Genes with strong patterns of acquisition of new variants such as *RB1* and *PIK3CA* tended to lose relatively few clones on treatment (Fig. 4C and D). In contrast, *ESR1* mutations showed substantial variation through treatment, with frequent loss and gain of different mutations through treatment (Fig. 4E and F; Supplementary Fig. S14), and high levels of *ESR1* polyclonality (13). Patients commonly had a different combination of *ESR1* mutations detectable at EOT compared with day 1 (Fig. 4F; Supplementary Fig. S14), and only 35.6% of *ESR1* variants detected at any time point were detected at both and thus maintained on treatment (42/118). This pattern of polyclonal flux observed in *ESR1* mutations supports the observation that individual *ESR1* mutations mark individual tumor subclones (Fig. 1), demonstrating the frequent clonal selection pressure provided by treatment.

Copy-Number Profiles Remain Predominantly Consistent through Treatment

We next assessed copy-number variation in plasma. Exome copy-number profiles ($n = 14$) were largely consistent between day 1 and EOT on palbociclib plus fulvestrant (Supplementary Figs. S18 and S19), contrasting with the clonal evolution observed in single-nucleotide variants (Fig. 1). Loss of 13q, encompassing the *RB1* locus, was lost in 6 of 14 (42.9%) patients at day 1 and 5 of 16 (31%) patients at EOT, with the majority of these being present at day 1 (4/5, 80%; Supplementary Fig. S20). There was no change in these findings with incremental reduction in the bin size, to investigate for large intragenic deletions in *RB1*.

To expand copy-number profile assessment beyond the exome sequencing, we assessed a larger set of matched pairs of day 1 and EOT samples from both treatment groups using the targeted sequencing panel that assessed loss of *RB1, PTEN,* and *CDKN2A,* tumor purity, and assessment of copy number in 12 genes commonly gained in breast cancer (Methods). In total, 324 samples were sequenced to assess copy number with median 1,329× coverage, comprising 163 day 1 samples and 154 paired EOT samples (Supplementary Figs. S21 and S22).

As assessing copy number in plasma DNA, and in particular copy-number loss, is highly dependent on having sufficient tumor purity, only the subset of samples with at least 20% tumor purity was used for assessment of losses. Of the day 1 samples, 37 had estimated ≥20% purity, with 51 EOT samples having ≥20% purity, yielding 17 patients for paired analysis (Supplementary Fig. S23). There was an association between number of sites of disease and tumor content >10% ($P = 0.039$, Cochran–Armitage test). Loss of *RB1* was identified in 6 of 37 patients (16.2%) in day 1 samples and 14 of 51 patients (27.4%) with EOT samples ($P = 0.30$, Fisher exact test). Among these losses, it was also possible to identify subgenic deletions with our approach (Supplementary Fig. S22; Supplementary Table S5). In EOT samples, we identified 3.8% (2 of 51) subgenic deletions, one of these also having a paired day 1 sample with the loss, suggesting these deletions preexisted and were not acquired during treatment. In the 17 samples with paired >20% purity, there was no evidence for selection of *RB1* loss on treatment (Supplementary Fig. S24; $P = 0.25$, McNemar test), although this analysis was limited by sample size. Consistent copy number through treatment was also observed for *PTEN* and *CDKN2A* (Supplementary Fig. S24).

Copy-number gain data at day 1 and EOT were assessed in those samples with >10% tumor purity and were largely consistent with the spectrum seen in primary breast cancer, with amplifications identified in *CCND1, MYC,* and *FGFR1*, without evidence for selection or loss at EOT in the 43 samples with paired purity >10% (Supplementary Fig. S25). Two patients acquired *FGFR2* amplification at EOT (Supplementary Fig. S25). There were no patients with acquired *CCNE1* or *CCNE2* amplification at EOT.

Selection of Genetic Variants Occurs Late on Palbociclib plus Fulvestrant

To investigate clinical factors that associated with selection of mutations on treatment, we explored the relationship between time on treatment (PFS) and acquisition of a new mutation at EOT (Methods) in patients on both palbociclib plus fulvestrant (Fig. 5) and placebo plus fulvestrant (Supplementary Fig. S26). The presence of any acquired mutation at the EOT was associated with longer PFS compared with patients who did not acquire a mutation (Fig. 5A; median 14.3 months acquired vs. 5.5 months not acquired; log-rank $P = 0.0018$; Supplementary Figs. S27 and S28), suggesting that new mutations were more likely to arise in patients who had been on treatment longer. This trend was also seen separately for acquired *ESR1* mutations (Supplementary Fig. S29; median PFS 13.7 acquired vs. 7.4 months not acquired; log-rank $P = 0.032$) and *PIK3CA* mutations (Supplementary Fig. S30; median 12.7 acquired vs. 9.2 months not acquired, log-rank $P = 0.34$), mutations in these two genes comprising the majority of the acquired mutations (Fig. 5B). There were too few acquired *RB1* mutations to meaningfully assess a relationship with PFS (Supplementary Fig. S31). Assessment of baseline clinicopathologic characteristics with patients who had acquired a mutation revealed some evidence of an association with the presence of bone metastases ($P = 0.013$, $q = 0.15$; Supplementary Table S6).

DISCUSSION

CDK4/6 inhibitors in combination with endocrine therapy now represent the standard of care for advanced hormone receptor–positive breast cancer, but little is known

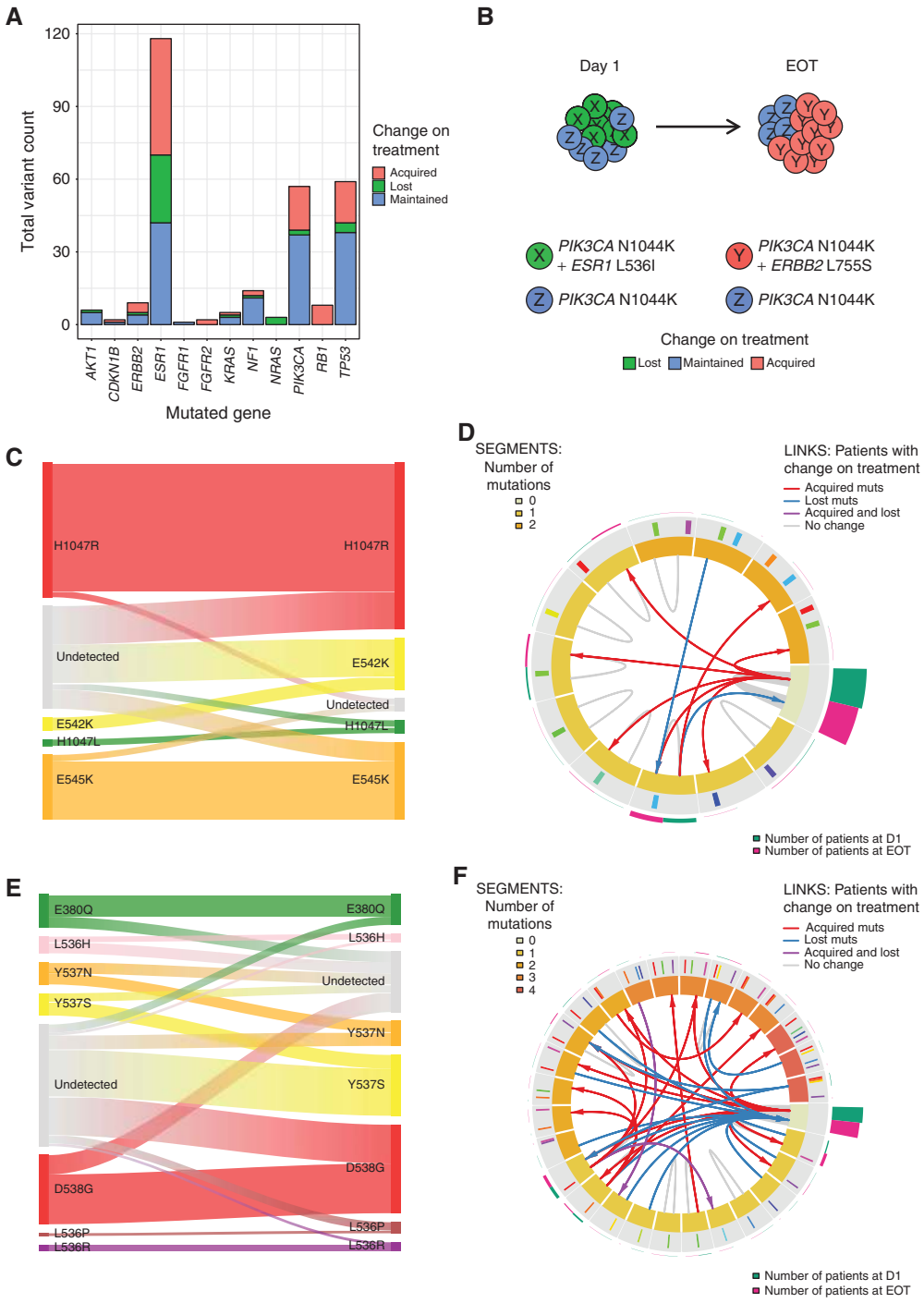

Figure 4. Clonal evolution of breast cancer driver genes through treatment. **A,** Individual variants for each gene in the treatment groups combined ($n = 195$), split by variants maintained between day 1 and EOT, lost over the course of treatment, or acquired during treatment. A number of patients had polyclonal variants in a single gene, particularly *ESR1*. The majority of *TP53* acquired variations are accounted for by a single patient acquiring 8 separate new variants at EOT (see also Supplementary Fig. S9). **B,** Cartoon with data from patient 237 illustrating subclonal selection on treatment. A clonal *PIK3CA* mutation and an *ESR1*-mutant subclone are detectable at day 1. Over the course of treatment, the *ESR1*-mutant subclone present at day 1 is lost, with acquisition of a new *ERBB2*-mutant subclone. **C,** Sankey diagram to illustrate changes in individual *PIK3CA* mutations through treatment in both treatment groups combined. Polyclonal mutations from a single patient are displayed separately. Only two *PIK3CA* mutations detected at day 1 are undetectable at EOT, one from a patient with the other polyclonal mutation detected at EOT. **D,** Clonal state diagram to illustrate changes in *PIK3CA* polyclonality through treatment, with each individual patient represented once at day 1 and EOT. Inner track demonstrates clonal states, representing different combinations of *PIK3CA* mutations indicated by segments of the circle. The middle tracks show individual mutations in the clonal states. The outer track shows the number of patients with that specific combination of mutations at day 1 (green bar) and EOT (purple bar). The central arrows show changes between day1 and EOT. The plot incorporates data from both treatment arms ($n = 195$). **E,** Sankey diagram to illustrate changes in individual *ESR1* mutations through treatment in both treatment groups combined. **F,** Clonal state diagram to illustrate changes in *ESR1* polyclonality through treatment, with each individual patient represented once at day 1 and EOT; see the legend in **D**.

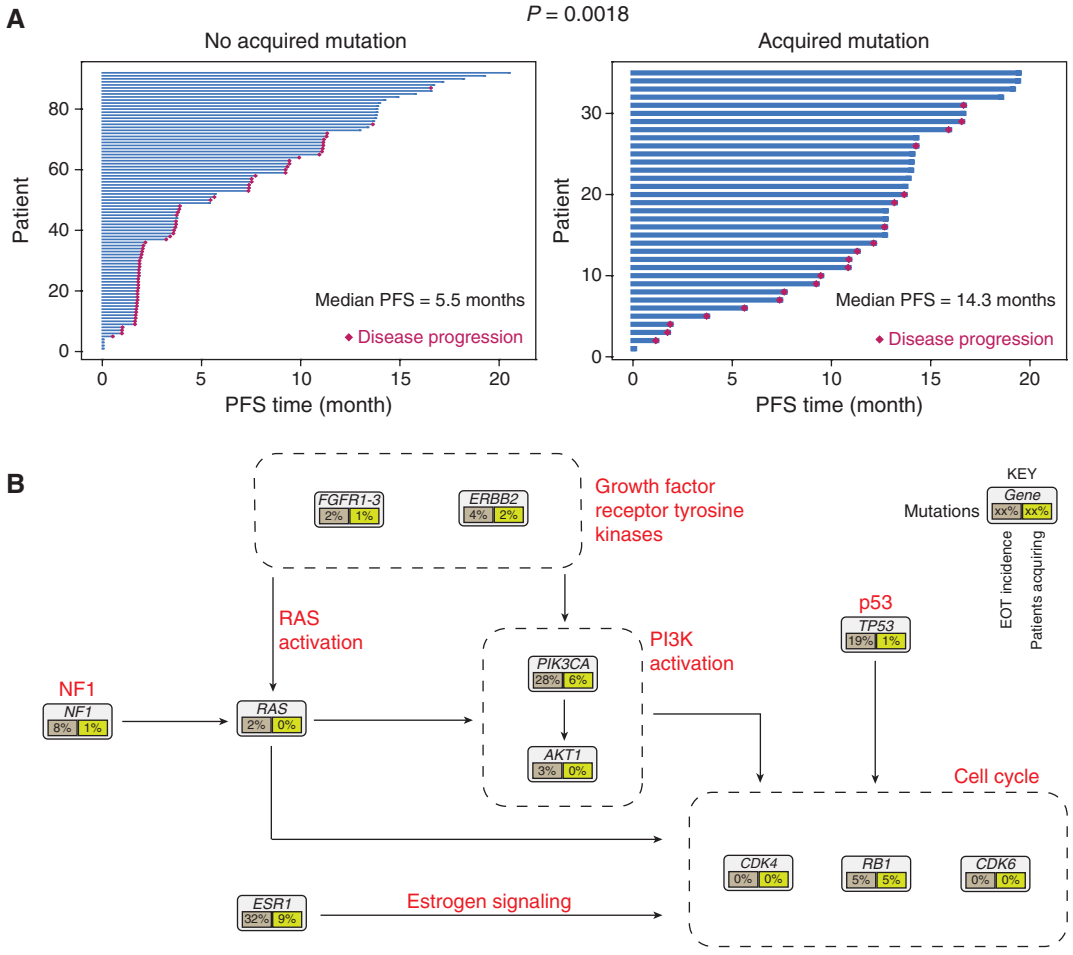

Figure 5. New driver mutations are selected late on treatment with palbociclib plus fulvestrant. **A,** Swimmers plot of patients with paired sequencing data who received palbociclib plus fulvestrant ($n = 127$), comparing PFS between patients with any acquired driver mutation at EOT ($n = 35$) versus patients who did not acquire a new driver mutation ($n = 92$). *P* value calculated using log rank. **B,** Genetic landscape of breast cancer progressing after palbociclib plus fulvestrant treatment. Each box shows the percentage of patients with a mutation identified at EOT (gray) and the subset of these patients who have newly acquired a mutation by EOT (yellow) for each gene. Patients with different mutations in a gene between day 1 and EOT are not counted as acquired. HR, hazard ratio; CI, confidence interval.

about mechanisms of resistance to these treatments. Here, we study the evolution of genetic mechanisms of resistance to palbociclib plus fulvestrant in these breast cancers and show that clonal evolution is frequent in response to therapy. Three main changes in driver genes are identified. Acquired mutations in *RB1* occur relatively infrequently and are often subclonal, detected in the plasma of 5% of patients after palbociclib plus fulvestrant (Fig. 2A–C). Acquired driver mutations in growth factor receptors and signal transduction pathways are frequently detected in patients treated with palbociclib plus fulvestrant, occurring in 39 of 127 (30.7%) patients in total (Figs. 2C and 5D), dominated by 6% of these patients acquiring *PIK3CA* mutations, with 9% more patients having at least 1 *ESR1* mutation by EOT compared with day 1 (Fig. 5D). Evolution of *ESR1* mutations is observed, with selection of *ESR1* Y537S as the variant most likely promoting resistance to fulvestrant in the combination (Figs. 3A and 4E). Conversely, acquisition or selection of the mutations examined in our panel was seen predominantly in patients with longer treatment duration. This suggests that patients with tumors intrinsically resistant to treatment less frequently acquire mutations, presumably due to the lack of selective pressure of treatment, and that other mechanisms of resistance may dominate in early progression.

Preclinical work has identified *RB1* mutations (9, 11) as a mechanism of resistance to CDK4/6 inhibition, consistent with the literature that functional RB is required for the efficacy of CDK4/6 inhibitors (18). Of these potential mechanisms of resistance, only mutations in *RB1* have been identified in the clinic, although their prevalence in a treated population is unknown (11). Condorelli and colleagues have recently reported 3 patients with *RB1* mutations following treatment with CDK4/6 inhibition, 2 of these receiving palbociclib with fulvestrant in the setting of previous endocrine treatment, and the other receiving ribociclib and letrozole as first-line treatment for advanced disease (11). With the advantages of analyzing an unbiased registration study, our

study confirms apparent positive selection of *RB1* aberrations on palbociclib plus fulvestrant, but demonstrates they are evident in only a minority of patients (Fig. 2A). In these patients, we identify polyclonal *RB1* aberrations, suggestive of phenotypic convergence under selective pressure, such as is seen with *ESR1* mutations in response to endocrine therapy (13, 19). Intriguingly, *RB1* mutations were selected only in tumors wild-type for *ESR1* mutations (Fig. 2D). Although we are unable to exclude a chance finding, this does possibly suggest that *RB1* mutations could be selected when fulvestrant efficacy is not compromised by *ESR1* mutation, suggesting divergent routes to resistance. Our finding of relatively uncommon *RB1* mutations is important in suggesting that subsequent lines of endocrine-based therapy have the potential to be active on progression, concurring with currently available postprogression clinical data (15).

With the exception of *RB1* mutations, there was no evident difference in acquired mutation profiles between the fulvestrant and palbociclib versus fulvestrant and placebo groups (Fig. 2C). This observation within the context of a randomized trial suggests that resistance to fulvestrant is a major genetic driver of resistance to combination therapy, possibly with tumors able to adapt to CDK4/6 inhibition without ER signaling suppressed. *ESR1* mutations are an important mechanism of resistance to aromatase inhibitors, with mutations in the ligand binding domain, particularly helix 12, resulting in a constitutively active protein (20, 21). Nevertheless, the detection of multiple resistant subclones at baseline did not predict palbociclib activity in PALOMA-3 (13). Our data suggest a significant proportion of *ESR1* mutations present at day 1 are lost on palbociclib plus fulvestrant, at least in part reflecting the high level of clonal evolution on therapy with loss of *ESR1* mutations reflecting loss of the sensitive subclone (Fig. 1C and G), with others emerging during subsequent fulvestrant treatment at the same rate and pattern in both treatment groups (Fig. 2C). We find evidence for positive selection of Y537S at EOT (Fig. 3A and D; Fig. 4E), this being the ligand binding domain mutation identified in preclinical studies as the most resistant to fulvestrant (22). This suggests separate, parallel evolution of mechanisms of resistance to the combination of palbociclib plus fulvestrant.

Further acquired driver mutations were observed in growth factor receptors and signal transduction pathways (Fig. 5D). *PIK3CA* mutations are important founding variants in ER-positive primary breast cancers (12) and remain clonally dominant in most metastatic breast cancers (23). We now identify that 6% of patients with no detectable *PIK3CA* mutations at day 1 acquire, or positively select, newly evident *PIK3CA* mutations at the EOT with palbociclib plus fulvestrant (Figs. 2C and 4A, C, and D), in particular E542K in this study (Supplementary Fig. S11). The prevalence of emergent *PIK3CA* mutations did not appear to differ between treatment groups (Supplementary Fig. S13), favoring the hypothesis that these are principally effecting fulvestrant resistance (24). Through exome sequencing, we identify a role for ABOPEC in driving clonal diversity and resistance to palbociclib plus fulvestrant (Fig. 1D and H; Supplementary Table S3). We note E542K is a potential APOBEC site, with the dominance of E542K potentially providing further evidence to support APOBEC mutagenesis in promoting genetic diversity in advanced ER-positive breast cancer (25, 26).

Our study also has potentially important findings in relation to the existing preclinical literature on mechanisms of resistance to CDK4/6 inhibitors. Prior preclinical work identified acquired amplification of *CCNE1* (9) or *CDK6* (10) in palbociclib- and abemaciclib-resistant models, respectively. We find no evidence that acquired *CCNE1* or *CDK4* amplification is relevant in the clinic, although we do note that ctDNA analysis is limited in analyzing copy number due to the challenge of low tumor purity. We partly address this limitation by adopting a novel targeted sequencing approach to allow concurrent assessment of purity and copy number, restricting copy-number analysis for gain to those tumors with at least 10% tumor purity, and loss to those with at least 20% tumor purity (Supplementary Figs. S21–S25). Our plasma tumor purity observations are comparable with the third of patients having >10% tumor content in the large breast cancer set reported in Adalsteinsson and colleagues (27), with the slightly higher rates of purity observed in our study (42% of day 1 samples, 68/163; and 53% of EOT samples, 82/154), perhaps due to be explained by all the samples being processed under the strict protocol mandated in the study. However, we emphasize that ctDNA analysis would be unlikely to detect many subclonal amplifications or losses. In addition, we find no evidence for gatekeeper mutations in *CDK4* or *CDK6* and can effectively exclude this from being a common mechanism of resistance (Fig. 2A).

Our study has a number of limitations. Making comparisons between longitudinal time points in ctDNA is difficult due to variations in tumor content—inability to identify mutations may be a result of absence of tumor DNA in plasma, or presence at a low level that falls into the sequencing noise. We mitigate this concern by conducting secondary analyses—analyzing baseline plasma with digital PCR for newly emergent mutations and performing a subset analysis of patients with known day 1 tumor content. The problem of purity is challenging particularly for assessing genomic loss, compounded for comparative analyses where confidence is required in the tumor content at more than a single time point. This may limit the investigation of *RB1* loss, and we suggest that tissue-based analysis will be required for a definitive analysis of copy number on progression. Although we analyzed 14 patients by paired exome sequencing, for discovery and to design our targeted panel, we cannot address whether there are rare acquired events not interrogated by our targeted panel. Additionally, we have interrogated relatively few EOT plasma samples from patients with over 2-year treatment duration, and so we are unable to address whether very late progression may have a different pattern of acquired mutations. Finally, we use the term "acquired" in this article to reflect a mutation detectable at EOT that was not detectable at day 1. It is very challenging to assess whether these mutations may have preexisted in the tumor prior to treatment in a minor and undetectable subclone. Investigating this exhaustively for Y537S with very high sensitivity digital PCR, we do detect at very low level some of the "acquired" and "lost" mutations at day 1 and EOT, respectively, but show that these are balanced between the two time points and do not significantly affect the comparative result (Fig. 3D).

Our study has important clinical implications for future therapeutic approaches in breast cancer. Resistance to fulvestrant is identified as a major driver of resistance to the combination of palbociclib plus fulvestrant. A number of potent oral selective estrogen receptor downregulators (SERD) are in clinical development, and our findings suggest that more potent targeting of the estrogen receptor has potential to improve on fulvestrant in combination with palbociclib. Oral SERDs should specifically address their clinical activity against *ESR1* Y537S. A number of targetable kinase mutations are enriched on palbociclib plus fulvestrant, with an approximate doubling of the number of detectable hotspot activating *ERBB2* mutations, activating *FGFR* mutations, and high-level acquired *FGFR2* amplifications, all of which invite precision medicine–guided therapeutic approaches after progression. Mutations in *PIK3CA* are selected through fulvestrant therapy, suggesting a greater role for PI3K inhibitors after therapy as well as the potential for triple combination therapy (ER, CDK4/6, PI3K) to prevent the outgrowth of resistant clones driven by acquired *PIK3CA* mutations.

Our work demonstrates the value of interrogating large registration trials with paired ctDNA analysis, demonstrating how ongoing clonal evolution in breast cancer drivers undermines palbociclib plus fulvestrant therapy, highlighting a potential role for APOBEC mutagenesis in promoting clonal evolution, and identifies rational therapeutic strategies that could improve efficacy of CDK4/6 inhibition.

METHODS

PALOMA-3 Study Design

The PALOMA-3 trial was a phase III, double-blind randomized controlled trial comparing palbociclib plus fulvestrant to placebo plus fulvestrant in patients with $ER^+/HER2^-$ advanced breast cancer. The trial recruited 521 patients randomized in a 2:1 ratio to receive oral palbociclib 125 mg daily, 3 weeks on, 1 week off, or matched placebo. All patients received fulvestrant 500 mg every 4 weeks. Premenopausal women received goserelin in addition. Patients were eligible if they had either progressed on endocrine treatment for advanced disease or progressed during or within 12 months following adjuvant endocrine therapy. The study was conducted in accordance with the Declaration of Helsinki and the principles of Good Clinical Practice. An institutional review board or equivalent approved the study at each participating site, with patients supplying written informed consent. The trial was registered as NCT01942135 at ClinicalTrials.gov.

Plasma Collection and Processing

Blood samples were collected at day 1 of treatment and EOT in EDTA blood collection tubes. These were centrifuged within 30 minutes at 1,500 to 2,000 × *g* before separation of the plasma and storage at −80°C and transfer to a central laboratory. Prior to extraction, plasma was centrifuged again at 3,000 × *g* for 10 minutes, and the supernatant was used for extraction. DNA extraction was performed using the Circulating Nucleic Acid kit (cat. #55114) from Qiagen. DNA was quantified using a TaqMan-based digital PCR assay against *RPPH1* from LifeTech (cat. #4403326). Buffy coat was extracted using the Qiagen Qiacube according to the manufacturer's instructions.

Digital PCR

Digital PCR experiments were performed with TaqMan probes in 20 μL reactions partitioned into 20,000 micelles in an oil and water emulsion using the Bio-Rad AutoDG system before undergoing PCR in a G Storm thermocycler. Prior to use, cycling conditions for each TaqMan assay were optimized using a thermal gradient and G blocks from Integrated DNA Technologies. Droplets were read on a Bio-Rad QX200 and concentrations calculated by fitting a Poisson model to the data using Bio-Rad QuantaSoft version 1.4.0.99. Day 1 DNA samples were screened for *ESR1* mutations S463P (c.1387T>C), Y537N (c.1609T>A), E380Q (c.1138G>C), L536R (c.1607T>G), Y537C (c.1610A>G), D538G (c.1613A>G), and *PIK3CA* mutations E542K (c.1624G>A), E545K (c.1633G>A), H1047R (c.3140A>G), and H1047L (c.3140A>T) as previously described (13). For the purposes of exome sequencing, EOT samples were tested for a mutation with digital PCR only if a mutation was found in the matched day 1 sample to estimate purity. For purity estimates from digital PCR allele fractions, mutations were assumed to be heterozygous with a copy number of 2.

Exome Sequencing

Matched day 1 and EOT samples with adequate material (minimum 13 ng to preserve library complexity) and purity (10%) were selected for exome sequencing. Hybrid capture libraries were prepared using Agilent SureSelect V6 with paired-end sequencing performed on an Illumina HiSeq 2500 to a target depth of 150× for plasma and 50× for germline. Reads were aligned to the hg19 reference using BWA v0.7.12 (28), and duplicates were removed with Picard (v2.8.2) according to GATK best practices (28). Copy number was assessed using cnvkit v0.8.4 (29) and purity with ASCAT 2 (30). Variant calling between pairs was performed with MuTECT v1.1.7 (31), MuTECT2 (GATK v3.7), VarDict v1.5.0 (32), and between samples and the panel of germlines using MuTect2 and GATK. Variants were considered only if they had coverage of 40× and were identified by 2 callers. Clonality analysis was performed with PyClone (0.13.0; ref. 17), the mutational signature analysis with the R package deconstructSigs (33), and the chromosomal instability indices as described in Andor and colleagues (34). For samples without matched germline DNA, PyClone was used to identify and screen germline SNPs from paired analysis. For samples without matched germline DNA, putative SNPs were removed from analysis either using a variant allele fraction (VAF) cutoff < 0.4 or by comparing VAF in both EOT and day 1 samples. Copy-number profiles were compared using GISTIC (35). Additional diagrams and fish plots were produced using clonevol (36). Sequencing data are publicly available at the Sequencing Read Archive, using the accession number SRP157645.

Targeted Copy Number and Purity Panel

A 1729 amplicon custom panel was designed using the AmpliSeq designer software (Thermo Fisher Scientific) to allow combined copy-number and purity assessment. For purity assessment, the panel included approximately 1,000 SNPs with population prevalence over 20% in 8 chromosomal regions that commonly exhibit loss of heterozygosity in breast cancer: 16q24.3, 17p12, 8p23.2, 11q23.3, 22q13.31, 1p36.13, 6q27, and 3p21.31. Assessment of tumor purity was validated down to 10% by comparison with validated digital PCR assay allele fraction (Supplementary Table S7). For robust assessment of loss, a similar approach was used to include *RB1, CDKN2A* (p16), and *PTEN* with 119, 134, and 128 SNPs for each, respectively. For copy-number assessment, approximately 20 amplicons were sited in 11 genes commonly amplified in breast cancer and 19 reference genes identified from The Cancer Genome Atlas (TCGA; ref. 12) and METABRIC (37) data as being relatively copy-number invariant. Libraries were constructed with 1–3 ng input using the IonTorrent Library kit v2.0 (Thermo Fisher Scientific) and sequenced to a target depth of 1,000–2,000× on the Ion Proton using P1 chips. Reads were aligned using Torrent Suite software. Loss of heterozygosity was estimated using a bespoke pipeline that used a threshold of 5% for the presence of a β allele based on variance seen in germline material with a minimum of 15 informative SNPs (Supplementary Fig. S32; Supplementary Table S8) using an approach adopted

from previous CLONET analyses (38, 39). A minimum of 4 amplicons were used. Purity was estimated by assuming a single diploid clone with loss of heterozygosity, with this approach yielding similar estimates of purity to digital PCR (Supplementary Table S7) and CLONET (ref. 40; Supplementary Fig. S33), with reported profiles in the validated set matching the expected distribution from TCGA (Supplementary Fig. S34). Copy number was assessed using the OncoCNV (v6.8; ref. 41) package with calls based on normalized logR values obtained using thresholds of 0.24 for gain and −0.18 for loss. These thresholds were established using 3 standard deviations from the mean, derived from sequenced germline samples using the purity panel. To account for intergene variability within the panel, an additional z test with an α of 0.05 was performed against the local logR for all the samples. Copy-number estimates were adjusted for purity where purity exceeded the minimum threshold of 10%. Primers capturing *CCNE2* were included only for 226 of 324 samples, and so *CCNE2* was not assessable in the other 98 samples. *RB1* loss was defined as either evidence of heterozygous loss (normalized logR < −0.18 with or without evidence of LOH) or probable homozygous loss where the adjusted copy number was <1.

Targeted Gene Panel Sequencing

The AmpliSeq designer (Thermo Fisher Scientific) was used to create a 305 amplicon custom panel with amplicons covering the coding exons of *RB1, CDK4, CDK6, CDKN1A, CDKN1B, NF1*, exons 5–8 of *TP53*, and mutational hotspots in *ERBB2, PIK3CA, AKT1, ESR1, FGFR1, FGFR2*, and *FGFR3*. Two libraries were constructed for each sample with 1.5–5 ng of DNA per primer pool at each time point with the initial multiplex PCR of 22–24 cycles depending on input. One set of libraries were taken through the conventional IonTorrent Library kit v2.0 protocol, whereas the matched set was cleaned with AMPure XP (Beckmann Coulter) beads following FuPa digestion, and the library prep was completed using the KAPA Hyper Prep kit with dual-index adaptors without further PCR. The IonTorrent libraries were then sequenced to a target depth of 2,000× on a Proton with P1 chips. The custom libraries were sequenced on an Illumina HiSeq 2500 to target coverage of 15,000×. Sequencing reads were aligned and BAM files generated for the IonTorrent libraries using the Torrent Suite software and with BWA for the Illumina libraries. Sequencing artifact was removed with iDES (42) and manual curation with variants called from pileup only if present in both data sets above an allele fraction of 0.3% for hotspots, stopgains, and frameshifts and 0.5% for all other calls, with a minimum of 5 alternative reads. VarDict was used to call indels under the same constraints on both platforms, and torrent caller was used for IonTorrent libraries and Mutect2 for Illumina libraries. This approach was validated using dilutions of a blend of ctDNA (Supplementary Fig. S35).

Statistical Analyses

Kaplan–Meier survival analyses for PFS were performed with the log-rank test using a Cox proportional hazards model to obtain hazard ratios and 95% confidence intervals. Comparison of frequency of particular genomic aberrations in unpaired day 1 samples versus EOT was done using the Fisher exact test. Analysis of paired data between day 1 and EOT was performed using McNemar test with a continuity correction where required. Unless stated otherwise, all *P* values were two-sided with an α of 0.05. Statistical analyses were conducted using R version 3.4.3. To address potential undersampling at the day 1 time point, for the survival analysis comparing patients with and without an acquired mutation, mutations were included as acquired only if the variant calls in the Ion Torrent and Illumina libraries passed an additional statistical test. The proportions of alternative and reference reads between day 1 and EOT were compared using the Fisher exact test, with calls with only $P < 0.05$ in both libraries being included in the survival analysis. Of 60 patients with acquired mutations, 53 of 60 met these criteria and were included in the survival analysis. Survival analyses were conducted using the latest data cutoff from the trial (October 2015), in which the median PFS was 4.6 months for fulvestrant plus placebo and 11.2 months for palbociclib plus fulvestrant (15).

Disclosure of Potential Conflicts of Interest

B. O'Leary reports receiving a commercial research grant from Pfizer. X. Huang has ownership interest (including stock, patents, etc.) in Pfizer. F. André reports receiving commercial research support from Pfizer (research grant to the institution). S. Loibl reports receiving a commercial research grant from Pfizer and is a consultant/advisory board member for Pfizer and Novartis. S. Loi reports receiving a commercial research grant from Pfizer and other commercial research support from Novartis, BMS, Genentech, and Merck. M. Cristofanilli is a consultant/advisory board member for Novartis and Merus. C. Huang Bartlett is senior medical director at Pfizer and has ownership interest (including stock, patents, etc.) in the same. N.C. Turner is a consultant/advisory board member for Pfizer. No potential conflicts of interest were disclosed by the other authors.

Authors' Contributions

Conception and design: B. O'Leary, Y. Liu, S. Loi, I. Garcia-Murillas, C. Huang Bartlett, N.C. Turner
Development of methodology: B. O'Leary, R.J. Cutts, Y. Liu, S. Loi, I. Garcia-Murillas, C. Huang Bartlett
Acquisition of data (provided animals, acquired and managed patients, provided facilities, etc.): B. O'Leary, Y. Liu, S. Hrebien, K. Fenwick, F. André, S. Loi, C. Huang Bartlett
Analysis and interpretation of data (e.g., statistical analysis, biostatistics, computational analysis): B. O'Leary, R.J. Cutts, Y. Liu, S. Hrebien, X. Huang, F. André, S. Loibl, S. Loi, C. Huang Bartlett, N.C. Turner
Writing, review, and/or revision of the manuscript: B. O'Leary, R.J. Cutts, Y. Liu, S. Hrebien, X. Huang, F. André, S. Loibl, S. Loi, I. Garcia-Murillas, M. Cristofanilli, C. Huang Bartlett, N.C. Turner
Administrative, technical, or material support (i.e., reporting or organizing data, constructing databases): B. O'Leary, Y. Liu, S. Loi
Study supervision: S. Loi, I. Garcia-Murillas, N.C. Turner

Acknowledgments

We thank the patients, families, and trial staff who took part in the PALOMA-3 trial. We thank Francesca Demichelis and Alessandro Romanel for their help in performing the CLONET validation analyses, Irene Chong for assistance with MYC amplification validation by digital PCR, and Erle Holgersen for advice regarding the circos plots. This research was funded by The Medical Research Council (MR/N002121/1) and Breast Cancer Now with support from the Mary-Jean Mitchell Green Foundation and Pfizer. ICR-CTSU receives program grant funding from Cancer Research UK (grant C1491/A15955). We acknowledge National Institute for Health Research funding to the Royal Marsden and Institute of Cancer Research Biomedical Research Centre.

The costs of publication of this article were defrayed in part by the payment of page charges. This article must therefore be hereby marked *advertisement* in accordance with 18 U.S.C. Section 1734 solely to indicate this fact.

Received March 12, 2018; revised July 9, 2018; accepted September 6, 2018; published first September 11, 2018.

REFERENCES

1. Turner NC, Neven P, Loibl S, Andre F. Advances in the treatment of advanced oestrogen-receptor-positive breast cancer. Lancet 2016;389:2403–14.
2. Sherr CJ, Roberts JM. CDK inhibitors: positive and negative regulators of G1-phase progression. Genes Dev 1999;13:1501–12.

3. Goodrich DW, Wang NP, Qian Y-W, Lee EYHP, Lee W-H. The retinoblastoma gene product regulates progression through the G1 phase of the cell cycle. Cell 1991;67:293–302.
4. Harbour JW, Luo RX, Santi AD, Postigo AA, Dean DC. Cdk phosphorylation triggers sequential intramolecular interactions that progressively block Rb functions as cells move through G1. Cell 1999;98:859–69.
5. Sledge GW, Toi M, Neven P, Sohn J, Inoue K, Pivot X, et al. MONARCH 2: abemaciclib in combination with fulvestrant in women with HR+/HER2− advanced breast cancer who had progressed while receiving endocrine therapy. J Clin Oncol 2017;35:2875–84.
6. Goetz MP, Toi M, Campone M, Sohn J, Paluch-Shimon S, Huober J, et al. MONARCH 3: abemaciclib as initial therapy for advanced breast cancer. J Clin Oncol 2017;35:3638–46.
7. Finn RS, Martin M, Rugo HS, Jones S, Im S-A, Gelmon K, et al. Palbociclib and letrozole in advanced breast cancer. N Engl J Med 2016;375:1925–36.
8. Hortobagyi GN, Stemmer SM, Burris HA, Yap Y-S, Sonke GS, Paluch-Shimon S, et al. Ribociclib as first-line therapy for HR-positive, advanced breast cancer. N Engl J Med 2016;375:1738–48.
9. Herrera-Abreu MT, Palafox M, Asghar U, Rivas MA, Cutts RJ, Garcia-Murillas I, et al. Early adaptation and acquired resistance to CDK4/6 inhibition in estrogen receptor-positive breast cancer. Cancer Res 2016;76:2301–13.
10. Yang C, Li Z, Bhatt T, Dickler M, Giri D, Scaltriti M, et al. Acquired CDK6 amplification promotes breast cancer resistance to CDK4/6 inhibitors and loss of ER signaling and dependence. Oncogene 2017;36:2255–64.
11. Condorelli R, Spring L, O'Shaughnessy J, Lacroix L, Bailleux C, Scott V, et al. Polyclonal RB1 mutations and acquired resistance to CDK 4/6 inhibitors in patients with metastatic breast cancer. Ann Oncol 2018;29:640–5.
12. The Cancer Genome Atlas Network. Comprehensive molecular portraits of human breast tumours. Nature 2012;490:61–70.
13. Fribbens C, O'Leary B, Kilburn L, Hrebien S, Garcia-Murillas I, Beaney M, et al. Plasma ESR1 mutations and the treatment of estrogen receptor–positive advanced breast cancer. J Clin Oncol 2016;34:2961–8.
14. Cristofanilli M, Turner NC, Bondarenko I, Ro J, Im S-A, Masuda N, et al. Fulvestrant plus palbociclib versus fulvestrant plus placebo for treatment of hormone-receptor-positive, HER2-negative metastatic breast cancer that progressed on previous endocrine therapy (PALOMA-3): final analysis of the multicentre, double-blind, phase 3 randomised controlled trial. Lancet Oncol 2016;17:425–39.
15. Turner NC, Andre F, Cristofanilli M, Verma S, Iwata H, Loi S, et al. Abstract P4-22-06: Treatment postprogression in women with endocrine-resistant HR+/HER2− advanced breast cancer who received palbociclib plus fulvestrant in PALOMA-3. 2017. P4–22 p.
16. Nik-Zainal S, Morganella S. Mutational signatures in breast cancer: the problem at the DNA level. Clin Cancer Res 2017;23:2617–29.
17. Roth A, Khattra J, Yap D, Wan A, Laks E, Biele J, et al. PyClone: statistical inference of clonal population structure in cancer. Nat Methods 2014;11:396.
18. Finn R, Dering J, Conklin D, Kalous O, Cohen D, Desai A, et al. PD 0332991, a selective cyclin D kinase 4/6 inhibitor, preferentially inhibits proliferation of luminal estrogen receptor-positive human breast cancer cell lines in vitro. Breast Cancer Res 2009;11:R77.
19. Chandarlapaty S, Chen D, He W, Sung P, Samoila A, You D, et al. Prevalence of ESR1 mutations in cell-free DNA and outcomes in metastatic breast cancer: a secondary analysis of the BOLERO-2 clinical trial. JAMA Oncol 2016;2:1310–5.
20. Toy W, Shen Y, Won H, Green B, Sakr RA, Will M, et al. ESR1 ligand-binding domain mutations in hormone-resistant breast cancer. Nat Genet 2013;45:1439–45.
21. Jeselsohn R, Buchwalter G, De Angelis C, Brown M, Schiff R. ESR1 mutations-a mechanism for acquired endocrine resistance in breast cancer. Nat Rev Clin Oncol 2015;12:573–83.
22. Toy W, Weir H, Razavi P, Lawson M, Goeppert AU, Mazzola AM, et al. Activating *ESR1* mutations differentially affect the efficacy of ER antagonists. Cancer Discov 2017;7:277–87.
23. Pereira B, Chin S-F, Rueda OM, Vollan H-KM, Provenzano E, Bardwell HA, et al. The somatic mutation profiles of 2,433 breast cancers refine their genomic and transcriptomic landscapes. Nat Commun 2016;7:11479.
24. Mayer IA, Arteaga CL. PIK3CA activating mutations: a discordant role in early versus advanced hormone-dependent estrogen receptor–positive breast cancer? J Clin Oncol 2014;32:2932–4.
25. Lefebvre C, Bachelot T, Filleron T, Pedrero M, Campone M, Soria J-C, et al. Mutational profile of metastatic breast cancers: a retrospective analysis. PLOS Med 2016;13:e1002201.
26. Savas P, Teo ZL, Lefevre C, Flensburg C, Caramia F, Alsop K, et al. The subclonal architecture of metastatic breast cancer: results from a prospective community-based rapid autopsy program "CASCADE." PLOS Med 2016;13:e1002204.
27. Adalsteinsson VA, Ha G, Freeman SS, Choudhury AD, Stover DG, Parsons HA, et al. Scalable whole-exome sequencing of cell-free DNA reveals high concordance with metastatic tumors. Nat Commun 2017;8:1324.
28. Van der Auwera GA, Carneiro MO, Hartl C, Poplin R, Del Angel G, Levy-Moonshine A, et al. From FastQ data to high confidence variant calls: the Genome Analysis Toolkit best practices pipeline. Curr Protoc Bioinformatics 2013;43:11.0.1–33.
29. Talevich E, Shain AH, Botton T, Bastian BC. CNVkit: genome-wide copy number detection and visualization from targeted DNA sequencing. PLoS Comput Biol 2016;12:e1004873.
30. Van Loo P, Nordgard SH, Lingjærde OC, Russnes HG, Rye IH, Sun W, et al. Allele-specific copy number analysis of tumors. Proc Natl Acad Sci U S A 2010;107:16910–5.
31. Cibulskis K, Lawrence MS, Carter SL, Sivachenko A, Jaffe D, Sougnez C, et al. Sensitive detection of somatic point mutations in impure and heterogeneous cancer samples. Nat Biotechnol 2013;31:213.
32. Lai Z, Markovets A, Ahdesmaki M, Chapman B, Hofmann O, McEwen R, et al. VarDict: a novel and versatile variant caller for next-generation sequencing in cancer research. Nucleic Acids Res 2016;44:e108.
33. Rosenthal R, McGranahan N, Herrero J, Taylor BS, Swanton C. deconstructSigs: delineating mutational processes in single tumors distinguishes DNA repair deficiencies and patterns of carcinoma evolution. Genome Biol 2016;17:31.
34. Andor N, Graham TA, Jansen M, Xia LC, Aktipis CA, Petritsch C, et al. Pan-cancer analysis of the extent and consequences of intratumor heterogeneity. Nat Med 2015;22:105.
35. Mermel CH, Schumacher SE, Hill B, Meyerson ML, Beroukhim R, Getz G. GISTIC2.0 facilitates sensitive and confident localization of the targets of focal somatic copy-number alteration in human cancers. Genome Biol 2011;12:R41.
36. Dang HX, White BS, Foltz SM, Miller CA, Luo J, Fields RC, et al. ClonEvol: clonal ordering and visualization in cancer sequencing. Ann Oncol 2017;28:3076–82.
37. Curtis C, Shah SP, Chin S-F, Turashvili G, Rueda OM, Dunning MJ, et al. The genomic and transcriptomic architecture of 2,000 breast tumours reveals novel subgroups. Nature 2012;486:346–52.
38. Carreira S, Romanel A, Goodall J, Grist E, Ferraldeschi R, Miranda S, et al. Tumor clone dynamics in lethal prostate cancer. Sci Transl Med 2014;6:254ra125.
39. Romanel A, Tandefelt DG, Conteduca V, Jayaram A, Casiraghi N, Wetterskog D, et al. Plasma AR and abiraterone-resistant prostate cancer. Sci Transl Med 2015;7:312re10.
40. Prandi D, Baca S, Romanel A, Barbieri C, Mosquera J-M, Fontugne J, et al. Unraveling the clonal hierarchy of somatic genomic aberrations. Genome Biol 2014;15:439.
41. Boeva V, Popova T, Lienard M, Toffoli S, Kamal M, Le Tourneau C, et al. Multi-factor data normalization enables the detection of copy number aberrations in amplicon sequencing data. Bioinformatics 2014;30:3443–50.
42. Newman AM, Lovejoy AF, Klass DM, Kurtz DM, Chabon JJ, Scherer F, et al. Integrated digital error suppression for improved detection of circulating tumor DNA. Nat Biotechnol 2016;34:547–55.